Hindawi
Advances in Civil Engineering
Volume 2023, Article ID 5731841, 12 pages
https://doi.org/10.1155/2023/5731841

Research Article

Experimental Study on the Flexural Behavior of Connected Precast Concrete Square Piles

Zhongji Dong,[1] **Faning Dang**,[2] **and Jun Gao**[2]

[1]*Xi'an Engineering Investigation & Design Research Institute of China, National Nonferrous Metals Industry, Co., Ltd., Xi'an 710054, China*
[2]*State Key Laboratory of Eco-Hydraulics in Northwest Arid Region, Xi'an University of Technology, Xi'an 710048, China*

Correspondence should be addressed to Faning Dang; dangfn@163.com

Received 12 November 2022; Revised 1 February 2023; Accepted 27 March 2023; Published 19 April 2023

Academic Editor: Danqing Song

Part of deep foundation pit support engineering needs to select connected precast concrete square piles (CPCSPs). Under the premise that the quality of precast concrete square piles (PCSPs) meets engineering requirements, the quality of CPCSPs becomes the key factor to ensure the safety of foundation pit support structures. This paper puts forward a new connection technology of CPCSPs and carries out the flexural behavior experiment of unconnected precast concrete square piles (UPCSPs) and CPCSPs. The distribution of crack and strain on different surfaces of UPCSPs and CPCSPs are measured by carbon fiber composite strain sense optical cables, glass fiber composite strain sense optical cables, and fixed-point polyurethane strain sense optical cables. The anti-crack load, ultimate load, bending moment, and flexural deformation of UPCSPs and CPCSPs are measured. The experimental results of UPCSPs and CPCSPs are compared. The results show that the anti-crack strength of CPCSPs is greatly increased while the flexural deformation of CPCSPs is decreased before the occurrence of crack. With the development of crack (failure stage), the outside areas of hoop steel plate exhibit cracks. At this moment, the strength of CPCSPs is no longer controlled by the strength of middle areas. The ultimate strength of CPCSPs is basically equivalent to that of UPCSPs. The ultimate bending moment of CPCSPs is higher than its design value (about 66%~76%). The selection of CPCSPs in the design of foundation pit support has good reliability.

1. Introduction

The foundation pit support technologies in China mainly include cast-in place pile, prestress anchor, diaphragm wall, inner support, (composite) soil nail wall, and SMW construction method. According to incomplete data statistics, the above traditional support forms [1–5] are chosen by more than 95% of foundation pits. However, with the development of society and the progress of technology, the problems of high cost, large construction space, long construction period, high energy consumption, and serious environment pollution of traditional support forms have become increasingly prominent. Precast concrete piles are more and more widely used in foundation pit support engineering because of their advantages in short construction period, reliable construction quality, high environmental protection, and economic benefits [6–10]. Due to the limits of production molds, transportation conditions, and piling equipment, the length of precast concrete piles generally does not exceed 15 m. Only the connected piles can meet the requirements for the embedded depth of deep foundation pit support structures.

In recent years, the bearing capacity performances of precast concrete piles are researched deeply by engineering and academic circles, and abundant research results have been obtained. The connection method of bonded steel plate weld for PHC piles in standard atlas was improved by Li et al. [11]. It was found that the mechanical performance, construction technology, and weld quality of improved connection joint had significantly improved compared to standard connection joint. On this basis, a new PHC uplift pile with hold-hoop connection method was proposed by

Zhang et al. [12, 13], which could significantly improve the pullout capacity of piles. The new mechanic-connection method was developed by Qi et al. [14]. It was found that the compressive and tensile capacity of mechanic-connection bamboo joint piles were significantly better than those of common prestress piles. The flexural behavior test of prestress concrete hollow square piles was carried out by Liu et al. [15], and it was found that the ultimate bending moment of weld joints met the requirement of inspection value. At the same time, the axial tensile tests on the internal buckle mechanic-connection joint of prestress concrete hollow square uplift piles were carried out by Fan et al. [16]. The comprehensive detection ways and judgment of deflect of precast square concrete piles were proposed by Zhang [17]. An extensive evaluation of capacity interpretation criteria was presented for driven precast concrete (PC) piles under axial compression loading by Marcos et al. [18]. The tensile and flexural behaviors of prestressed concrete square pile connection joint with resilient clamping were studied by Wang et al. [19, 20]. The flexural performance of prestressed concrete solid square piles and resilient clamping connections were studied by Xu et al. [21]. The experimental results indicated that the head of rebar and end of plate were the weak parts of piles. The full-scale flexural behavior experiments on the connection joints of composite reinforcement concrete precast square piles were carried out by Xu et al. [22]. The experimental results showed that the ultimate anti-bending capacity of connection joint was greater than that of pile shaft. Several widely used connection methods for precast concrete piles from economic benefit, service life, and field workload were summarized and compared by Ptuhina et al. [23]. The influence of topographic and geological conditions was considered by Song et al. [24–30].

At present, the research of connected piles is focus on the tensile and compressive strength of pile joints. There is little research on the flexural behavior of pile joints. The research work that has been carried out is either the small size or low bending performance of test specimens. As the precast concrete pile of foundation pit support, the main force condition is anti-bending. The technology requirements of connected piles are far higher than those of compression piles and tension piles. Therefore, it has an important engineering application value for foundation pit support to carry out the research on connection technologies and flexural behaviors of precast concrete piles. In this paper, a new connection technology for precast concrete square piles (PCSPs) is proposed. The tensile and compressive loads are transferred by plate groove weld, and the flexural loads are transferred by hoop steel plate. That is, the connection technology of hoop steel plate after welding plate groove is chosen to solve the complex force problems when PCSPs are used for foundation pit support. The relationships between flexural loads and displacement, ultimate load, and failure mode are researched by the flexural behavior test of full-scale CPCSPs and UPCSPs. The research results will provide an important theoretical basis for the design and application of CPCSPs.

2. Connection Technology of Anti-Bending Pile

In order to solve the complex force problems of tension, compression, and bending when PCSPs are used for foundation pit support, the connection technology of hoop steel plate after welding plate groove is chosen. Firstly, the bevel of plate groove is chamfered to 8 : 20 before welding, so as to increase the contact area of weld spot. Secondly, the hoop steel plate is made into two symmetrical "L" parts. The side length of pile section is 500 mm and 600 mm, respectively, and the length of hoop steel plate is 1000 mm and 1200 mm, respectively. After a layer of adhesive steel structural glue is evenly applied on the inner side of hoop steel plate, the hoop steel plate is firmly fixed at the connection joint of PCSPs with clamps. Finally, the hoop steel plate is firmly welded by groove weld technology.

The section size at the connection joint of PCSPs with side length of 500 mm is 480×480 mm, and the specification of hoop steel plate is $480 \times 480 \times 8$ mm. The section size at the connection joint of PCSPs with side length of 600 mm is 580×580 mm, and the specification of hoop steel plate is $580 \times 580 \times 8$ mm. The PCSP with side length of 600 mm is taken as an example, and the connection technology parameters of PCSPs are shown in Figures 1 and 2.

3. Flexural Test Scheme of Precast Concrete Square Connection Pile

The research on the tensile and compressive properties of CPCSPs is relatively mature. In this paper, the flexural behavior of CPCSPs is researched. The test includes two groups of PCSPs with different side lengths, and each group includes three CPCSPs and one UPCSP. Among them, Nos. 5-1, 5-2, 5-3, 6-1, 6-2, and 6-3 are CPCSPs, and 5A and 6A are UPCSPs. The lengths of piles are 7.0 m. The connection locations are located at the middle of PCSPs. The concrete strength of 6 CPCSPs is 43.7~54.7 MPa, and the average concrete strength is 49.08 MPa. The main parameters of CPCSPs and UPCSPs are shown in Table 1.

3.1. Load Device and Measurement Device of Test. The distribution beam, hydraulic jack, and manual oil pump are used for loading during test. The oil pressure gauge with accuracy of 0.4 level is used to measure pressure. The load device of test is shown in Figure 3. The digital dial indicators are used to measure the deflection of PCSPs and erected at the connection joint of PCSPs, with both sides of PCSPs with 0.8 m and 1.6 m away from connection joint, which are shown in Figure 4. The carbon fiber composite strain sense optical cables and glass fiber composite strain sense optical cables are used to measure the strain crack of piles. The fixed-point polyurethane strain sense optical cables are used to measure the crack of piles. The sense optical cables are, respectively, arranged on the top, upper and lower of front, and upper of back of piles, which are shown in Figure 5. The purpose that authors choose three different strain sense optical cables is to ensure the reliability of experimental

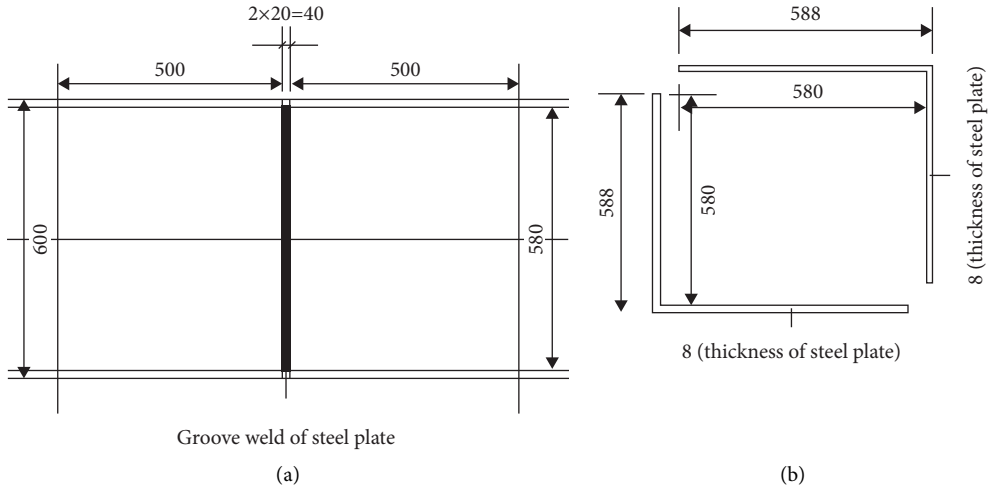

Figure 1: Schematic diagram of pile connection technology (unit: mm). (a) Connection location of pile. (b) Hoop steel plate.

Figure 2: Scene diagram of precast concrete square pile. (a) Precast concrete square pile. (b) Precast concrete square connection pile.

results. The main performances of measure instrument are shown in Table 2.

3.2. Load Method. Preload is loaded to eliminate virtual contact strain before test. The load increases from zero to 80% of estimated anti-crack bending moment according to the load with 20% of estimated anti-crack bending moment. The duration of each load level is 3 minutes. Then, the load increases from 80% to 100% of estimated anti-crack bending moment according to the load with 10% of estimated anti-crack bending moment. The duration of each load level is 3 minutes. During the test, observe whether there are cracks and record the distribution and development of cracks. If there is no crack at the load with 100% of estimated anti-crack bending moment, the load continues increasing until cracks appear according to the load with 10% of estimated anti-crack bending moment. The duration of each load level is 3 minutes. Then, the load continues increasing to the ultimate state of PCSPs according to the load with 10% of estimated anti-crack bending moment. The duration of each load level is 3 minutes. Observe and record all data.

3.3. Anti-Crack Load and Ultimate Load. It is considered to be the limit state of PCSPs when any of the following conditions occur. The crack width of piles reaches 1.5 mm. The tensile rebar is broken. The location of weld is broken or detached. The concrete in compression zone is failure. The load cannot increase or remain stable.

The anti-crack load is determined by following ways. When the crack occurs at the first time during loading, the previous load level is taken as the anti-crack load. When the crack occurs at the first time within the required duration of load level, the average value of the current load level and previous load level is taken as the anti-crack load. When the crack occurs at the first time after the required duration of load, the current load level is taken as the anti-crack load.

The ultimate load is determined by following ways. When the ultimate state is reached during loading, the previous load level is taken as the ultimate load. When the ultimate state is reached within the required duration of load level, the average value of the current load level and previous load level is taken as the ultimate load. When the ultimate state is reached after the required duration of load, the current load is taken as the ultimate load.

Before the test, the state of PCSPs is checked. All PCSPs are complete without crack. During the test, each PCSP is loaded to the ultimate state. The test results are as follows.

4. Test Results and Analysis

4.1. Distribution Law of Crack. During the test, each PCSP shows cracks. 5-1 and 5A are taken as examples to illustrate the distribution law of cracks in CPCSP and UPCSP, which are shown in Figures 6 and 7.

Figure 6 shows the crack distribution sketch of 5A and 5-1 under the last load level. Most cracks of piles are similar to the inversive splay, which is consistent with the stress state of

Table 1: Main parameters of precast concrete square pile.

Number of pile	Side length (mm)	Pile length (mm)	Pile shaft reinforcement	End plate	Concrete strength grade of pile shaft
5A 5-1 5-2 5-3	500	7	The main reinforcement is 12Φ12.6. The stirrup is Φ6.5. The distance between stirrups within 1.0 m at both ends of pile is 50 mm, and the rest of space is 75 mm.	480 × 480 × 20 mm (Q235 ordinary hot-rolled steel plate)	C40
6A 6-1 6-2 6-3	600	7	The main reinforcement is 20Φ12.6. The stirrup is Φ6.5. The distance between stirrups within 1.0 m at both ends of pile is 50 mm, and the rest of space is 75 mm.	580 × 580 × 20 mm (Q235 ordinary hot-rolled steel plate)	C40

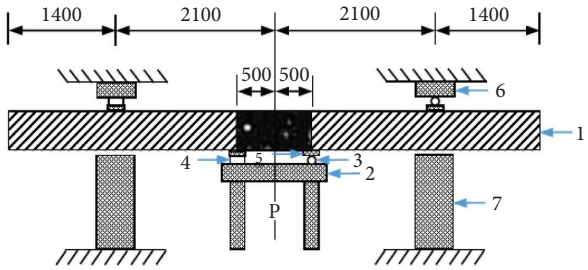

Figure 3: Schematic diagram of load equipment, where 1 is the CPCSP; 2 is the distribution beam; 3 is the rolling hinge support; 4 is the fixed hinge support; 5 is the bottom plate; 6 is the reaction pier after loading; and 7 is the protection pier before loading.

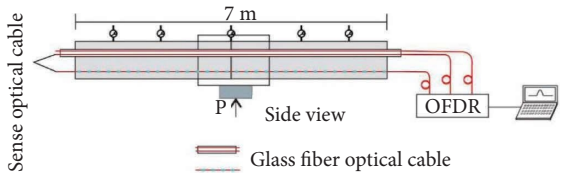

Figure 4: Layout of optical cable on the surface of CPCSP.

Table 2: Main performance of measurement instrument.

Name	Type	Range	Degree of accuracy
Digital dial indicator	MFX-50	50 mm	0.01 mm
Carbon fiber composite strain sense optical cable	NZS-DSS-C09(CF)	$\pm 15000\,\mu_\varepsilon$	$1\,\mu_\varepsilon$
Glass fiber composite strain sense optical cable	NZS-DSS-C09(GF)	$\pm 15000\,\mu_\varepsilon$	$1\,\mu_\varepsilon$
Fixed-point polyurethane strain sense optical cable	NZS-DSS-C08	$\pm 15000\,\mu_\varepsilon$	$1\,\mu_\varepsilon$

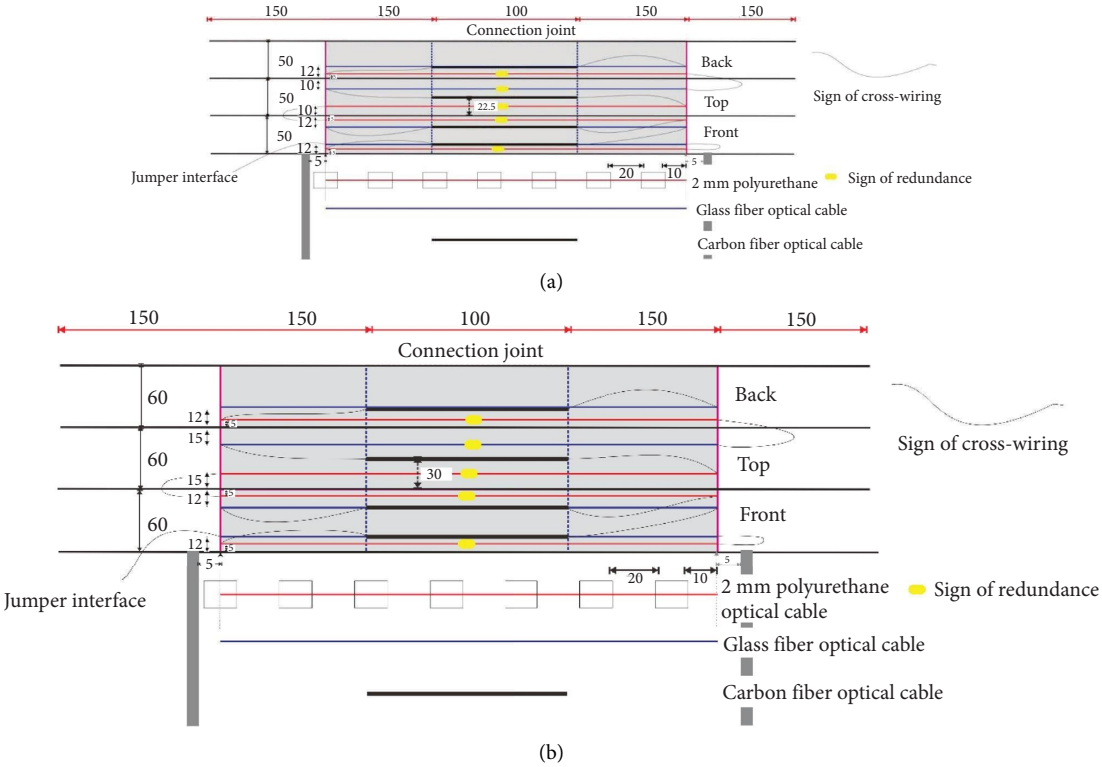

Figure 5: Actual layout of optical cable on the surface of CPCSP. (a) 500 mm. (b) 600 mm.

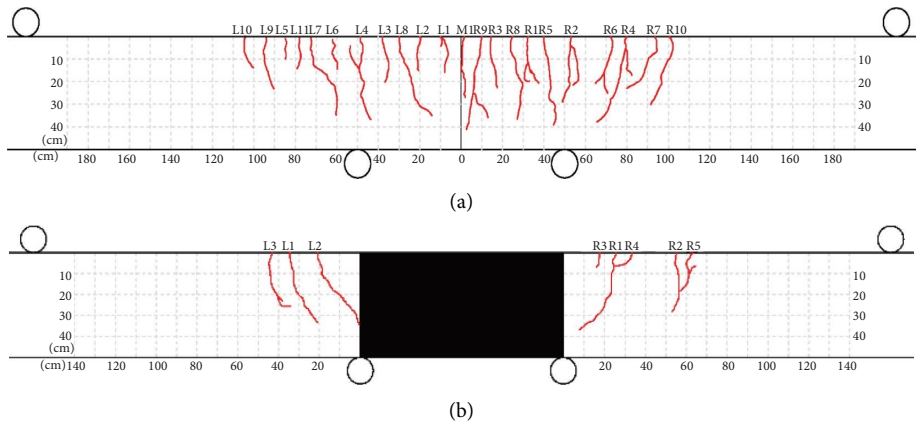

Figure 6: Actual distribution sketch of cracks in CPCSP and UPCSP. (a) 5A. (b) 5-1.

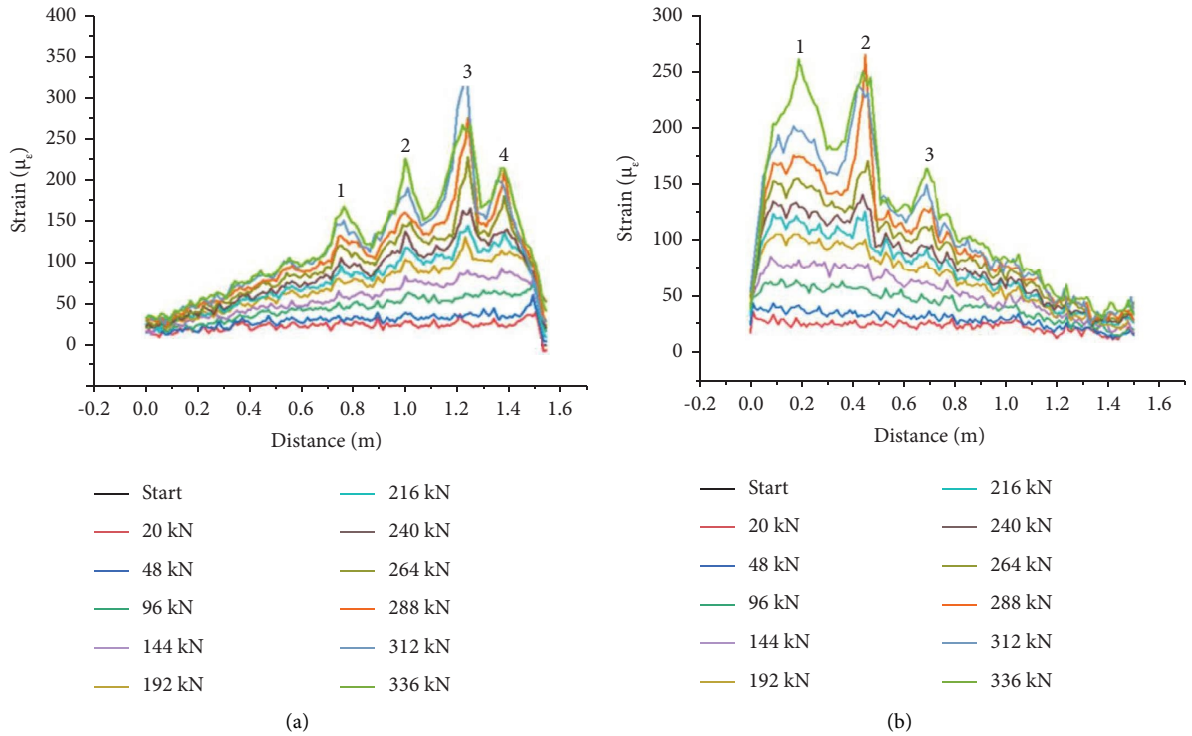

Figure 7: Test diagram of crack distribution law on left and right sides of 5-1. (a) Left side. (b) Right side.

piles with upper side under tension and lower side under compression. The crack density at the left side of 5A is 1.0/10 cm, and the crack density at the right side of 5A is 1.1/10 cm. The crack density at the left side of 5-1 is 0.7/10 cm, and the crack density at the right side of 5-1 is 0.8/10 cm. In comparison, the crack density of CPCSPs is significantly lower than that of UPCSPs, which is the main reason that the flexural deformation ability of UPCSPs is weakened.

Figure 7 shows the test crack distribution law of 5-1. There are 4 obvious strain peaks on the left side of 5-1 and 3 obvious strain peaks on the right side of 5-1. The experimental results show that the number and location of cracks are basically consistent with those of actual cracks. During the test, cracks first appeared at the middle of UPCSPs, while the middle of CPCSPs is the connection joint, which is co-affected by hoop steel plate and adhesive steel glue. The ductility and crack of CPCSPs are enhanced and reduced, respectively, by the coordination deformation of steel plate and concrete. The experimental results of other groups are similar to those of this test and will not be repeated.

4.2. Distribution Law of Stress and Strain. Since the stress state of each CPCSP is relatively consistent during the loading, 5-1 is also taken as an example to explore the stress and strain distribution law of CPCSPs. The experimental results are shown in Figures 8–10.

Figure 8 shows the strain diagram of glass fiber optical cable on the top, back, and front of 5-1. Before the load of 360 kN, the change of strain is small (within 200 μ_ε). The

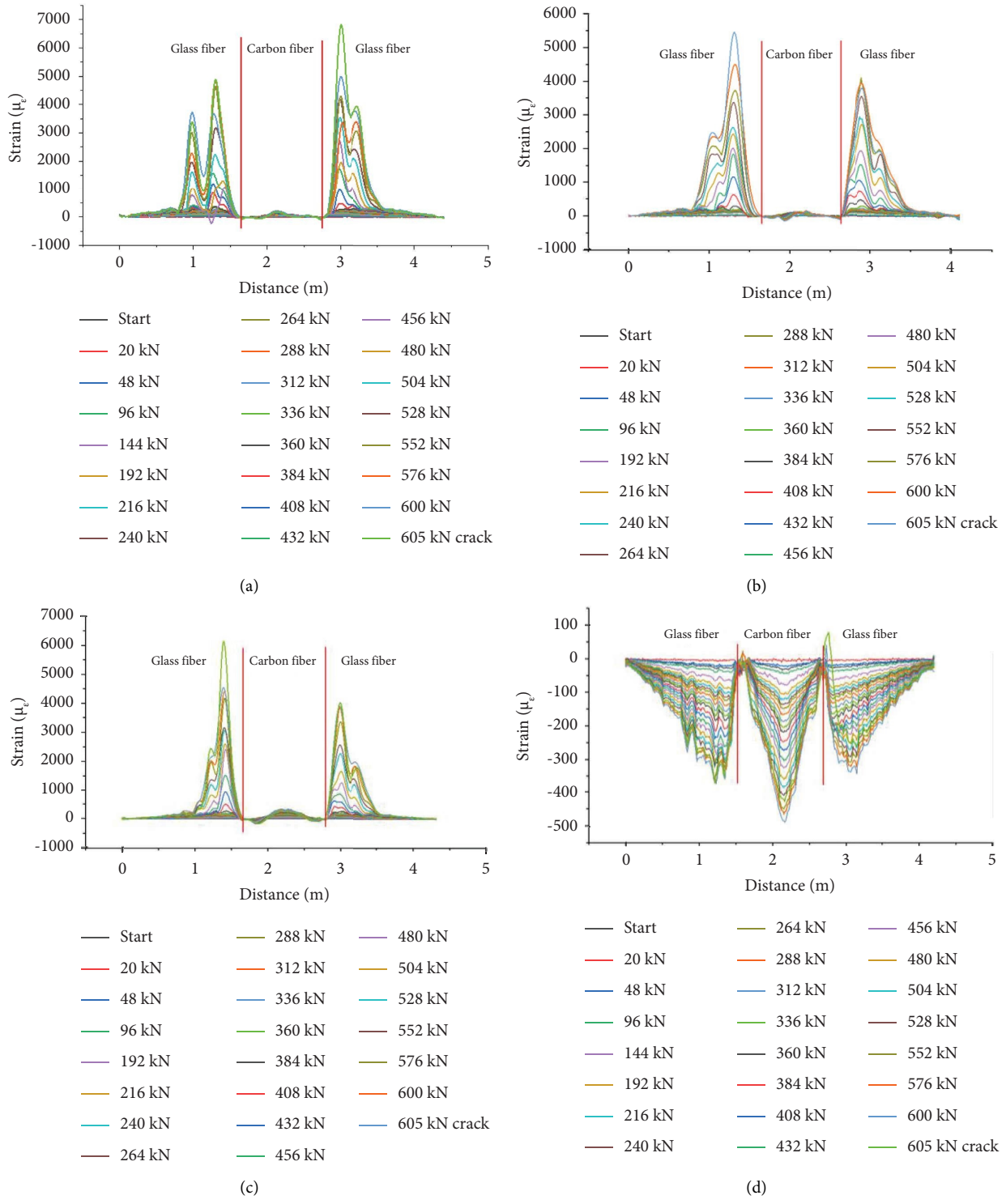

Figure 8: Strain diagram of glass fiber optical cable on the top, back, and front of 5-1. (a) Top. (b) Back. (c) Upper of front. (d) Lower of front.

stress is also small, and the crack is in the initial development stage. With the increase of load, the crack also starts to develop significantly after the load of 360 kN. The strain and stress increase significantly, and the stress concentration appears. In terms of whole 5-1, the stress at both ends is zero, and the stress increases gradually from both ends to connection joint. The stress on the top, upper of front, and back is positive, which is in tensile state. The stress on the lower of front is negative, which is in compressive state.

Figure 9 shows the strain diagram of polyurethane optical cable on the top, back, and front of 5-1. The test results are relatively consistent with the strain diagram of

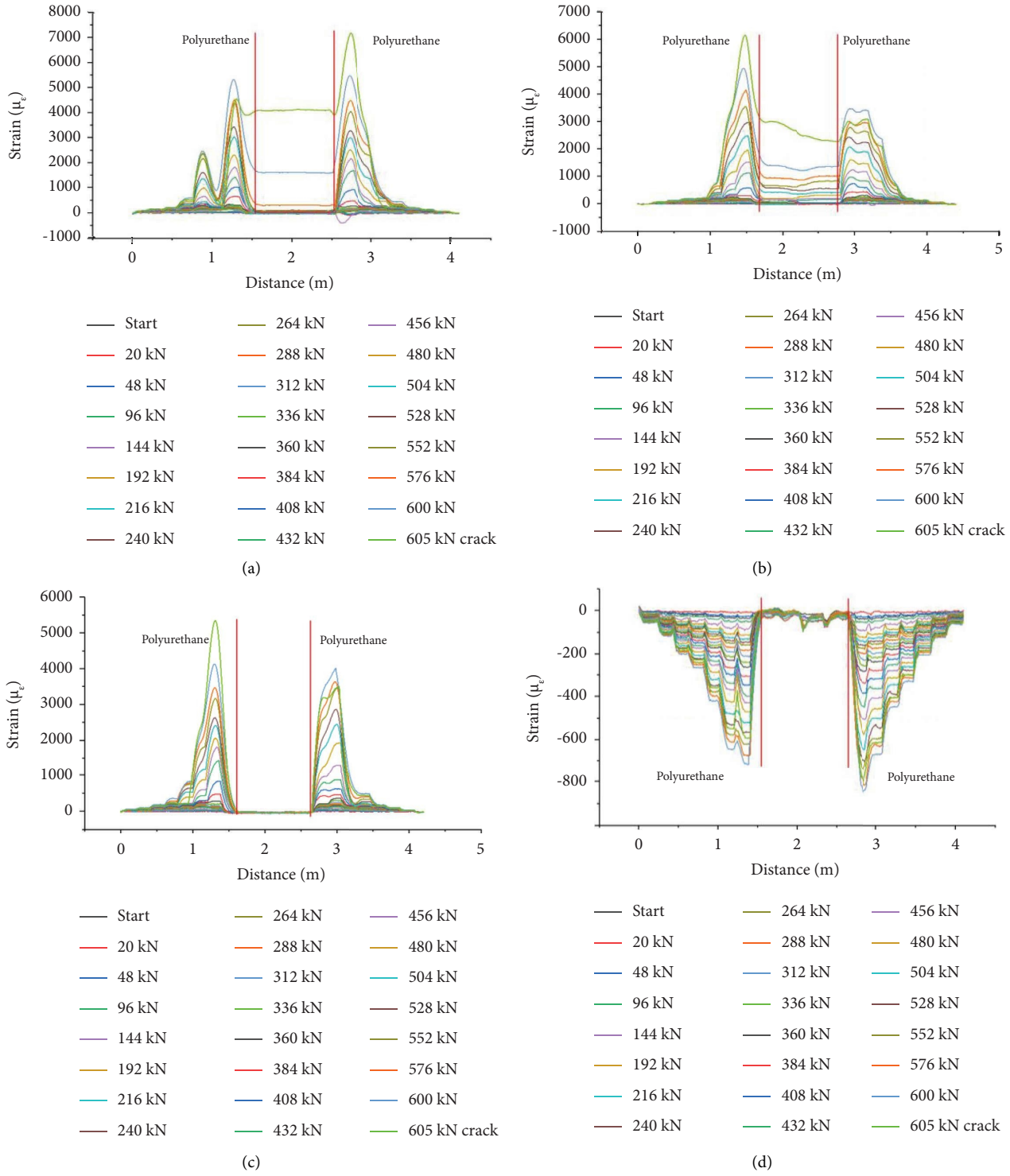

Figure 9: Strain diagram of polyurethane optical cable on the top, back, and front of 5-1. (a) Top. (b) Back. (c) Upper of front. (d) Lower of front.

glass fiber. Before the load of 360 kN, the change of strain is small. The stress is small, and the crack is in the initial development stage. With the increase of load, the crack starts to develop significantly after the load of 360 kN. The strain and stress also increase significantly. In terms of whole 5-1, the strain at both ends is zero, and the strain increases gradually from both ends to connection joint. The strain on the top, upper of front, and back is positive, which is in tensile state. The strain on the lower of front is negative, which is in compressive state.

Figure 10 shows the strain diagram of carbon fiber optical cable on the top (Figure 10 is the strain diagram of

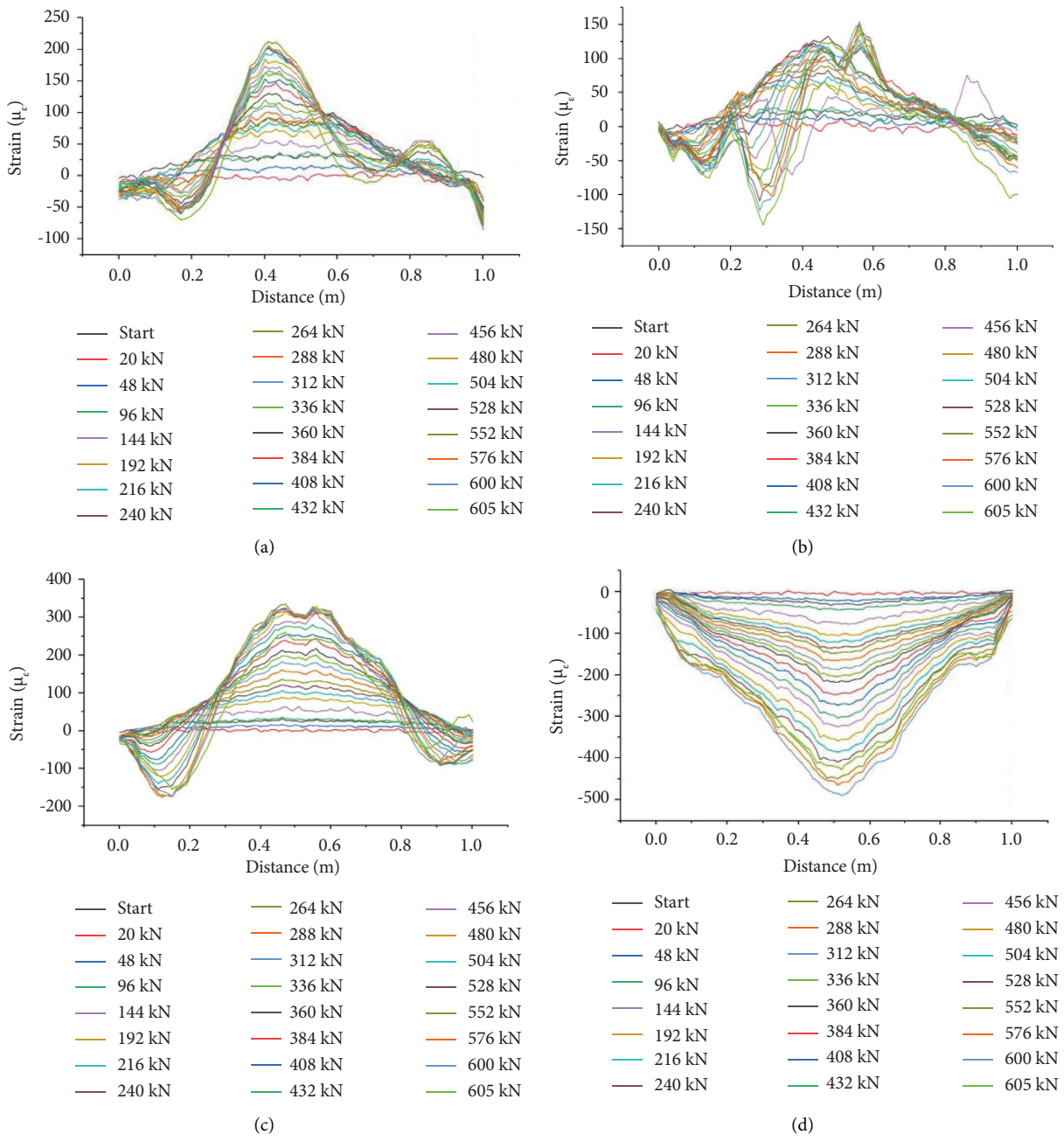

Figure 10: Strain diagram of carbon fiber optical cable on the top, back, and front of 5-1 (a) Top. (b) Back. (c) Upper of front. (d) Lower of front.

carbon fiber optical cable in the middle of Figure 8), back, and front of 5-1. The strain at the middle of connection joint is relatively large and concentrated, and the strain at both sides of connection joint is relatively small. In addition, the strain on the top, back, and front (except the lower of front) of the middle of connection joint is positive, which is in tension state. The strain at both sides of connection joint is negative, which is in compression state.

In summary, the pile has a tensile effect on the top, back, and front of hoop steel plate before the load of 144 kN, and the hoop steel plate is in tensile state. After the load of 144 kN and with the increase of load, the pile has a compressive effect on the back and upper of front of hoop steel plate, and the hoop steel plate is in compressive state. The pile has a downward tensile effect on the both sides for the top of hoop steel plate, and the hoop steel plate is in tensile state.

4.3. Comparison of Flexural Behavior between UPCSP and CPCSP. The anti-crack load, ultimate load, bending moment, and flexural deformation measured by tests are shown in Table 3. According to the test results of three CPCSPs with the side length of 500 mm (Nos. 5-1~5-3), the

Table 3: Anti-crack load, ultimate load, bending moment, and flexural deformation.

Number of pile	State of pile before test	Anti-crack load (kN)	Anti-crack bending moment (kN·m)	Maximum anti-crack flexural deformation (mm)	Ultimate load (kN)	Ultimate bending moment (kN·m)	Maximum ultimate flexural deformation (mm)	Design value of bending moment (kN·m)
5A	Complete without crack	332	257.9	16.36	577	454.7	40.95	260
6A		455	353.0	5.78	845	—	10.00	490
5-1		348	270.7	12.41	576	453.1	40.42	
5-2		396	309.1	12.08	576	453.1	30.90	260
5-3		444	347.5	21.56	600	472.3	49.46	
6-1		552	430.6	13.67	1072	846.6	40.42	
6-2		528	411.4	34.10	1056	833.8	39.17	490
6-3		552	430.6	11.99	975	769.0	47.94	

range of anti-crack load is 348~444 kN, and the average value is 396 kN. The range of anti-crack bending moment and maximum anti-crack flexural deformation is 270.7~347.5 kN·m and 12.08~21.56 mm, respectively, and the average value is 309.1 kN·m and 15.35 mm, respectively. The range of ultimate load is 576~600 kN, and the average value is 584 kN. The range of ultimate bending moment and maximum ultimate flexural deformation is 453.1~472.3 kN·m and 30.90~49.46 mm, respectively, and the average value is 459.5 kN·m and 40.26 mm, respectively. According to the test results of one UPCSP with the side length of 500 mm (No. 5A), the anti-crack load is 332 kN, and the anti-crack bending moment and maximum anti-crack flexural deformation are 257.9 kN·m and 16.36 mm, respectively. The ultimate load is 577 kN, and the ultimate bending moment and maximum ultimate flexural deformation are 454.7 kN·m and 40.95 mm, respectively. It can be seen that the anti-crack load and anti-crack bending moment of CPCSPs are greater than those of UPCSPs, and their value is increased by 19.28% and 19.85%, respectively. The ultimate load, ultimate bending moment, and maximum anti-crack or ultimate flexural deformation of CPCSPs and UPCSPs are basically equivalent. The strength and deformation characteristics of test are consistent with the results of mechanical theory analysis (the maximum tensile stress occurs in the middle of piles and at the top of cross section; because of the coordinated deformation of hoop steel plate and the pile concrete, the anti-bending strength and anti-crack ability of CPCSPs are enhanced, and its flexural deformation is weakened before the occurrence of crack). Therefore, the anti-crack strength of CPCSPs is greatly increased while the flexural deformation of CPCSPs is decreased. With the development of cracks, the outside areas of hoop steel plate show cracks. At this moment, the strength of CPCSPs is no longer controlled by the strength of middle areas, so it is shown that the ultimate strength of CPCSPs is basically equivalent to that of UPCSPs.

According to the test results of three CPCSPs with the side length of 600 mm (Nos. 6-1~6-3), the range of anti-crack load is 528~552 kN, and the average value is 544 kN. The range of anti-crack bending moment and maximum anti-crack flexural deformation is 411.4~430.6 kN·m and 11.99~13.67 mm (the maximum anti-crack flexural deformation of 6-2 is not accepted), respectively, and the average value is 424.2 kN·m and 12.83 mm, respectively. The range of ultimate load is 975~1072 kN, and the average value is 1034 kN. The range of ultimate bending moment and maximum ultimate flexural deformation is 769.0~846.6 kN·m and 40.42~47.94 mm, respectively, and the average value is 816.5 kN·m and 44.18 mm, respectively. According to the test results of one UPCSP with the side length of 600 mm (No. 6A), the anti-crack load is 455 kN, and the anti-crack bending moment is 353.0 kN·m. 6A shows crack under the load level of 520 kN. The test equipment produces deformation when the load reaches 845 kN, and the test is terminated. It is seen that the anti-crack load and ultimate load of CPCSPs are greater than those of UPCSPs, which again shows that the anti-bending strength of CPCSPs has been improved.

Table 4: Detailed data of flexural deformation (unit: mm).

Number of piles	No. 1	No. 2	No. 3	No. 4	No. 5
5A	23.88	34.52	40.95	36.99	24.52
6A	10	5.27	7.63	4.93	9.06
5-1	22.63	32.4	40.42	40.38	30.11
5-2	16.53	25.59	30.9	25.28	16.54
5-3	36.19	46.7	49.46	43.41	30.88
6-1	23.24	33.23	40.42	35.51	23.66
6-2	44.22	51.42	39.17	42.86	34.33
6-3	24.04	38.84	47.94	37.25	24.29

The flexural deformations of CPCSPs and UPCSPs are shown in Table 4. With the increase of load, the flexural deformation increases gradually. Except for 6-2 and 6A, which are affected by the deformation of simply supported beams, the flexural deformation at the center of other piles is greater than that of other positions. The maximum flexural deformation of 5-1~5-3 is between 30.90 and 49.46 mm, and the average value is 40.26 mm. The maximum flexural deformation of 5A is 40.95 mm. The maximum flexural deformation of 6-1 and 6-3 is 40.42 and 47.94 mm, respectively, and the average value is 44.19 mm. In summary, the anti-bending strength of CPCSPs is greater than that of UPCSPs.

5. Conclusions

The following conclusions are mainly obtained by experimental study on the flexural behavior of CPCSPs and UPCSPs:

(1) Most cracks of piles are similar to the inversive splay, which is consistent with the stress state of piles with upper side under tension and lower side under compression. The crack density of CPCSPs is significantly lower than that of UPCSPs

(2) The anti-crack bending moment of CPCSPs is about 19.85%~20.17% higher than that of UPCSPs before the occurrence of crack. The anti-crack strength of CPCSPs is greatly increased while the flexural deformation of CPCSPs is decreased. With the development of crack (failure stage), the outside areas of hoop steel plate exhibit cracks. At this moment, the strength of CPCSPs is no longer controlled by the strength of middle areas, so it is shown that the ultimate strength of CPCSPs is basically equivalent to that of UPCSPs.

(3) The ultimate bending moment of CPCSPs is not lower than that of UPCSPs and is about 66%~76% higher than its bending moment design value. Therefore, the selection of CPCSPs in the design of foundation pit support has good reliability.

Data Availability

The data used to support the findings of this study are included within the article.

Conflicts of Interest

The authors declare that they have no conflicts of interest.

Acknowledgments

This research was supported by the National Natural Science Foundation of China (grant nos. 51979225 and 51679199), the Key Research and Development Project of Shaanxi Province (2018SF-388), and the Special Research Projects of Shaanxi Provincial Department of Education (21JK0793).

References

[1] X. L. Huang, M. D. Liu, J. Y. Li, X. D. Zhou, and J. M. ten Cate, "Chemical composition of Galla chinensis extract and the effect of its main component(s) on the prevention of enamel demineralization in vitro," *International Journal of Oral Science*, vol. 4, no. 3, pp. 146–151, 2012.

[2] J. Xu, S. F. Yang, and H. Y. Wu, "Monito-ring and numerical analysis of pile-anchor supporting structure for deep and large foundation," *Journal of Xi'an University of Architecture and Technology*, vol. 51, no. 4, pp. 517–524, 2019.

[3] P. Lin, P. Liu, G. Ankit, and Y. J. Singh, "Deformation monitoring analysis and numerical simulation in a deep foundation pit," *Soil Mechanics and Foundation Engineering*, vol. 58, no. 1, pp. 56–62, 2021.

[4] T. Li, Y. W. Yang, and Y. Q. Zhou, "Analytical solution of horizontal displacement of retaining structures in deep foundation pit during dismantling inner support," *Chinese Journal of Rock Mechanics and Engineering*, vol. 41, no. 1, pp. 3021–3032, 2022.

[5] L. Z. Wang, B. He, Y. Hong, Z. Guo, and L. Li, "Field tests of the lateral monotonic and cyclic performance of jet-grouting-reinforced cast-in-place piles," *Journal of Geotechnical and Geoenvironmental Engineering*, vol. 141, no. 5, Article ID 06015001, 2015.

[6] L. Cai, S. D. Liang, and M. Gu, "Application of high reinforced prestressed concrete compounded pipe piles in deep foundation pit," *Geotechnical Investigation & Surveying*, vol. 46, no. 12, pp. 25–29, 2018.

[7] Z. P. Wang, "Discussion on connection of precast concrete square pile with high anti-pulling capacity," *Building Structure*, vol. 49, no. 2, pp. 846–849, 2019.

[8] D. J. Seo, D. M. Kang, H. G. Lee, and D. Y. Moon, "An experimental study on lateral load resistance of a wall structure composed of precast concrete and H-pile," *Journal of The Korea Institute for Structural Maintenance and Inspection*, vol. 24, no. 3, pp. 9–17, 2020.

[9] S. F. Zhao, G. L. Huang, and S. Q. Ma, "Application of precast concrete pipe piles in a deep excavation project," *Chinese Journal of Geotechnical Engineering*, vol. 36, no. 1, pp. 91–96, 2014.

[10] X. Y. Zhang, X. C. Chen, Y. Wang, D. Mingbo, and L. Jinhua, "Quasi-static test of the precast-concrete pile foundation for railway bridge construction," *Advances in Concrete Condtruction*, vol. 10, no. 1, pp. 49–59, 2020.

[11] W. X. Li, Y. R. Wan, and Q. B. Liu, "Design and experimental study on a new connection between PHC up lift pile segments of the Expo Theme Pavilion," *Journal of Building Structures*, vol. 31, no. 5, pp. 86–94, 2010.

[12] Z. M. Zhang, J. Yu, and G. X. Zhang, "Contrastive experimental analysis of bearing behaviors of PHC pile and precast square piles," *Rock and Soil Mechanics*, vol. 29, no. 11, pp. 3059–3065, 2008.

[13] Y. Guo, W. Cui, and F. B. Chen, "Analysis and experimental study of a PHC uplift pile with hold-hoop connection," *Chinese Journal of Geotechnical Engineering*, vol. 35, no. 2, pp. 1007–1010, 2013.

[14] J. L. Qi, P. H. Zhou, X. L. Yang, and Z. D. Zhou, "Application of mechanical-connection bamboo joint piles in the coastal soft soil foundation," *Building Structure*, vol. 44, no. 1, pp. 73–76, 2014.

[15] F. R. Liu, L. Jia, and C. Li, "The test study on welding joint flexural bearing capacity of prestressed concrete hollow square pile," *Journal of Wuhan University of Technology*, vol. 30, no. 5, pp. 105–108, 2008.

[16] Q. J. Fan, G. L. Huang, and H. L. Miao, "Computational analysis and experimental study on a new connection between segments of square uplift piles," *Chinese Journal of Geotechnical Engineering*, vol. 35, no. 2, pp. 1011–1015, 2013.

[17] X. W. Zhang, "Comprehensive detection ways and judgement of deflects of precast square concrete piles," *Building structure*, vol. 34, no. 4, pp. 48–50, 2004.

[18] M. C. M. Marcos, Y. J. Chen, and F. H. Kulhawy, "Evaluation of compression load test interpretation criteria for driven precast concrete pile capacity," *KSCE Journal of Civil Engineering*, vol. 17, no. 5, pp. 1008–1022, 2013.

[19] Y. F. Wang, G. Chen, and Q. B. Xu, "Study on tensile behavior of prestressed concrete square pile connection joint with

resilient clamping," *Journal of Disaster Prevention and Mitigation Engineering*, vol. 38, no. 6, pp. 1003–1011, 2018.

[20] J. W. Zhou, Y. F. Wang, and S. F. Gong, "Study on flexural behavior of prestressed concrete square pile connection joint with resilient clamping," *Building structure*, vol. 27, no. 13, pp. 121–127+133, 2020.

[21] Y. S. Xu, Z. F. Chen, J. Fan, Z. Li, K. Zhang, and X. Tu, "Study on the flexural performance of prestressed concrete solid square piles and resilient clamping connections," *KSCE Journal of Civil Engineering*, vol. 27, no. 1, pp. 285–298, 2022.

[22] Q. B. Xu, G. Chen, and J. F. He, "Flexural performance experiment of concrete of connection joint for composite reinforcement concrete prefabricated square piles," *Journal of Zhejiang University (Science Edition)*, vol. 51, no. 7, pp. 1300–1308, 2017.

[23] I. Ptuhina, R. Alzhanova, A. Akhatuly, and V. Maier, "Comparative analysis of pile joints," *Advanced Materials Research*, vol. 1082, pp. 270–276, 2014.

[24] D. Q. Song, X. L. Liu, J. Huang, Y. Zhang, J. Zhang, and B. N. Nkwenti, "Seismic cumulative failure effects on a reservoir bank slope with a complex geological structure considering plastic deformation characteristics using shaking table tests," *Engineering Geology*, vol. 286, Article ID 106085, 2021.

[25] D. Q. Song, X. L. Liu, J. Huang, and J. Zhang, "Energy-based analysis of seismic failure mechanism of a rock slope with discontinuities using Hilbert-Huang transform and marginal spectrum in the time-frequency domain," *Landslides*, vol. 18, no. 1, pp. 105–123, 2020.

[26] D. Q. Song, X. L. Liu, B. Li, J. Zhang, and J. J. V. Bastos, "Assessing the influence of a rapid water drawdown on the seismic response characteristics of a reservoir rock slope using time-frequency analysis," *Acta Geotechnica*, vol. 16, no. 4, pp. 1281–1302, 2021.

[27] D. Q. Song, Z. Chen, L. H. Dong, G. Tang, K. Zhang, and H. Wang, "Monitoring analysis of influence of extra-large complex deep foundation pit on adjacent environment: a case study of Zhengzhou City, China," *Geomatics, Natural Hazards and Risk*, vol. 11, no. 1, pp. 2036–2057, 2020.

[28] Y. Xue, J. Liu, P. G. Ranjith, F. Gao, H. Xie, and J. Wang, "Changes in microstructure and mechanical properties of low-permeability coal induced by pulsating nitrogen fatigue fracturing tests," *Rock Mechanics and Rock Engineering*, vol. 55, no. 12, pp. 7469–7488, 2022.

[29] Y. Xue, P. G. Ranjith, F. Gao, Z. Zhang, and S. Wang, "Experimental investigations on effects of gas pressure on mechanical behaviors and failure characteristic of coals," *Journal of Rock Mechanics and Geotechnical Engineering*, vol. 15, no. 2, pp. 412–428, 2023.

[30] Y. Xue, S. Liu, J. Chai et al., "Effect of water-cooling shock on fracture initiation and morphology of high-temperature granite: application of hydraulic fracturing to enhanced geothermal systems," *Applied Energy*, vol. 337, Article ID 120858, 2023.